

Hybrid solar cells based on dye-sensitized nanoporous TiO₂ electrodes and conjugated polymers as hole transport materials

D. Gebeyehu^a, C.J. Brabec^{a,*}, N.S. Sariciftci^a, D. Vangeneugden^b, R. Kiebooms^b,
D. Vanderzande^b, F. Kienberger^c, H. Schindler^c

^aLinz Institute for Organic Solar Cells (LIOS), Physical Chemistry, Johannes Kepler University of Linz, Altenbergerstraße 69, A-4040 Linz, Austria

^bInstitute for Material Research, Division Organic and Polymer Chemistry, Limburg University, B-3590 Diepenbeek, Belgium

^cInstitute for Biophysics, Johannes Kepler University of Linz, Altenbergerstraße 69, A-4040 Linz, Austria

Received 6 November 2000; received in revised form 11 April 2001; accepted 18 May 2001

Abstract

Solid state dye-sensitized photovoltaic solar cells were fabricated using a three-layer concept. The hybrid devices consist of a transparent inorganic nanocrystalline titanium dioxide (nc-TiO₂) layer with a thickness of 2 μm as electron acceptor and for electron transport. A surface-adsorbed RuL₂(NCS)₂:2 TBA dye complex (where L = 2,2'-bipyridyl-4,4'-dicarboxylic acid; TBA = tetrabutylammonium) is utilized for light absorption and electron injection to the conduction band of TiO₂. For the transport of holes to the back contact electrode conjugated polymers are used, either a poly(3-octylthiophene) (P3OT), or a low band-gap thiophene–isothianaphthene-based copolymer (PDTI). These devices exhibit an overall energy conversion efficiency of approximately 0.16% under simulated solar irradiation (80 mW/cm²). Furthermore, we have investigated the surface network morphology of these film layers by atomic microscope (AFM) exploring strategies to improve the efficiency. © 2001 Elsevier Science B.V. All rights reserved.

Keywords: Photovoltaics; Photoelectrochemical solar cells; Dye-sensitized nc-TiO₂; Polythiophene and derivatives; Thiophene–isothianaphthene copolymers; Metal/semiconductor interfaces

1. Introduction

The regenerative photoelectrochemical solar cells based on photosensitization of nanocrystalline TiO₂ are regarded as a potentially low-cost alternative to conventional solid state devices since the 1991 report by the Lausanne group [1]. Dye-sensitized nanocrystalline TiO₂ solar cells (nc-DSCs) are based on a fundamentally different working principle than commercial solar cells based on conventional semiconductors. Briefly speaking, these cells consist of a nanoporous working electrode formed by a sintered film of TiO₂ semiconductor nanoparticles (ca. 10–30 nm in diameter) with a thickness of several micrometers which serves as electron acceptor and transport layer coated with a monolayer of a Ru-bipyridyl-based dye for light absorption and electron injection into the TiO₂ conduction band. An electrolyte solution, either acetonitrile or a mixture of ethylene/propylene carbonate containing the redox couple iodide/triiodide (I⁻/I₃⁻), serves as redox medium to

regenerate the photoexcited dye molecules by reduction. For the operation of the photoelectrochemical device, the counter electrode is sealed to the working photoelectrode with a spacer and the volume between the electrodes as well as the voids between the TiO₂ nanoparticles are filled with the electrolyte solution. Photovoltaic energy conversion efficiencies as high as 10–11% at AM 1.5 standard solar spectrum (i.e. 1000 W/m²) have been reported [2–4]. With respect to these promising results, much research has been directed toward improving the photocurrent and photovoltage by, for example, developing new sensitizers [5–19], increasing the light scattering properties of the film [20,21], suppressing the charge recombination [2,22], improving the interfacial energetics [23], and altering the particle morphology [3,24,25].

Although the nc-DSCs show excellent power conversion performance, their commercial applications is still limited due to stability problems (like evaporation of the electrolyte, degradation of the electrolyte or of the dye) as well as technological aspects of the large module production. Most commercial applications require efficient, large area multi-cell modules that are simple to construct and connect. The presence of a liquid electrolyte makes the manufacturing

* Corresponding author. Tel.: +43-732-2468-8766;
fax: +43-732-2468-8770.
E-mail address: christoph.brabec@jk.uni-linz.ac.at (C.J. Brabec).

process of multi-cell modules difficult because cells must be electrically connected yet chemically separated, preferably on a single substrate. Therefore, recent efforts in dye-sensitized TiO₂ solar cell research are more focusing on replacing the liquid electrolyte with solid state analog (i.e. by substituting with a hole conducting material) to eliminate practical problems with sealing and degradation.

Polymeric materials are of practical interest as replacements for the liquid electrolyte since they are inexpensive and can be tailored chemically to fit a wide range of technological purposes. However, for the filling of the nanoporous electrode several requirements must be fulfilled. The polymers cast from solutions must penetrate into the pores between the nanoparticles, and should form a good contact with the adsorbed dye. Thus, the average molecular weight (and size) of the polymeric material is essential. Various approaches have been reported in literature, like a polymer gel electrolyte that conduct ions [26], inorganic materials such as p-type CuI, CuSCN as well as organic hole conductors such as triphenyldiamine (TPD) or polypyrrole [27–31]. Bach et al. [32] used an amorphous, organic hole transport material (HTM) to replace the electrolyte, in which positive charges are transported by hopping processes and realized devices which showed under white light illumination at 9.4 mW/cm² an efficiency of ~0.74%.

Generally, p-type semiconducting polymers that accept holes from the dye cation are potential candidates for replacing the liquid electrolytes [27–30,32]. In this n-type TiO₂ semiconductor/Ru-dye/p-type polymeric semiconductor device configuration, the photoexcited dye molecules sandwiched between the two semiconductors inject electrons into the conduction band of TiO₂ and holes into the p-type polymer. In order to realize this, several requirements have to be fulfilled.

1. The p-type polymeric material must be highly transparent in the spectral range, where the dye absorbs light.
2. A method must be available for depositing a p-type polymeric material without dissolving or degrading the dye monolayer on TiO₂ nanocrystallites.
3. The excited state energy level of the dye (S*) should be located above the conduction band of TiO₂ and the ground state (S₀) must be below the upper edge of the valence band of the p-type polymeric material. This is essential for electron transfer from the excited dye molecule to the conduction band of TiO₂ and hole transfer to the valence band of the p-type polymeric material.
4. The charge transport mobilities of the p-type polymeric materials must be sufficiently high.

In principle, the dye can also be replaced by the semiconducting polymer layer, bringing together the function of light absorption and charge (hole) transport in a single material [33]. For such devices additional processes and parameters contribute to the overall efficiency, including the exciton lifetime and diffusion coefficient in the polymer [34],

the rate of interfacial charge separation and recombination, the mobilities of charge carriers, and the wavelength dependence of photocarrier generation. In such a device the polymer fulfills the combined function as a sensitizer and as a hole transport layer. This implies a number of additional requirements for the polymer component as light absorbing layer.

1. A large exciton diffusion length.
2. A high efficiency of the electron transfer from the polymer layer into TiO₂.

At present, one of the major drawbacks of using polymer films in the photovoltaic devices, is the small exciton diffusion length. This parameter determines to what extent photons, which are not absorbed directly at the photoactive interface, contribute to the electrical output. According to [33] the value of for exciton diffusion was found to be 20 nm for a spin-coated film. On the other hand, in [35,36] an exciton diffusion length in the range of 5–20 nm has been reported. Several semiconducting polymers like poly(3-octylthiophene) (P3OT) (as demonstrated in this work); poly(bithiophene) (PBT); and poly(3-methylthiophene) (P3MT) could be used directly as a sensitizer of the nanocrystalline TiO₂. The photoinduced charge separation at the interface of the polymer and inorganic semiconductor provides interesting opportunities for application in photovoltaic device [37,38]. Furthermore, photoinduced absorption (PIA) and photoinduced ESR experiments demonstrated that nanocrystalline titanium dioxide (nc-TiO₂) acts as an efficient electron acceptor for poly(*p*-phenylenevinylene) and polythiophene derivatives [39]. From spectroscopy, the photoinduced charge transfer from conjugated polymer into TiO₂ [35–39] has been found to be comparable with the ultrafast (<100 fs) charge transfer from conjugated polymers to fullerenes.

In this work, we demonstrate that conjugated semiconducting polymers can be successfully adopted to concept of nanocrystalline TiO₂ solar cells, replacing the electrolyte as well as the dye.

2. Experimental

All devices were produced on 2.5 cm by 1.5 cm transparent conducting oxide (indium tin oxide, ITO) or fluorine-doped tin oxide (SnO₂:F) covered glass substrates with an active area of 5 mm². Fig. 1 shows the device configuration of a hybrid solid state solar cell together with the chemical structures of the materials used. The materials used are: poly(methyl methacrylate) (PMMA, supplied by Aldrich), P3OT (supplied by Neste Oy, *M_w* ~80.000 g/mol), three different thiophene–isothianaphthene-based copolymers (PDTI: further denoted as DV-032 (*M_w* ~7600 g/mol), DV-036 (*M_w* ~6200 g/mol), and DV-053 (*M_w* ~2500 g/mol), synthesized by oxidative polymerization with FeCl₃ [40]) and RuL2(NCS)₂:2 TBA (supplied by Solaronix Co.

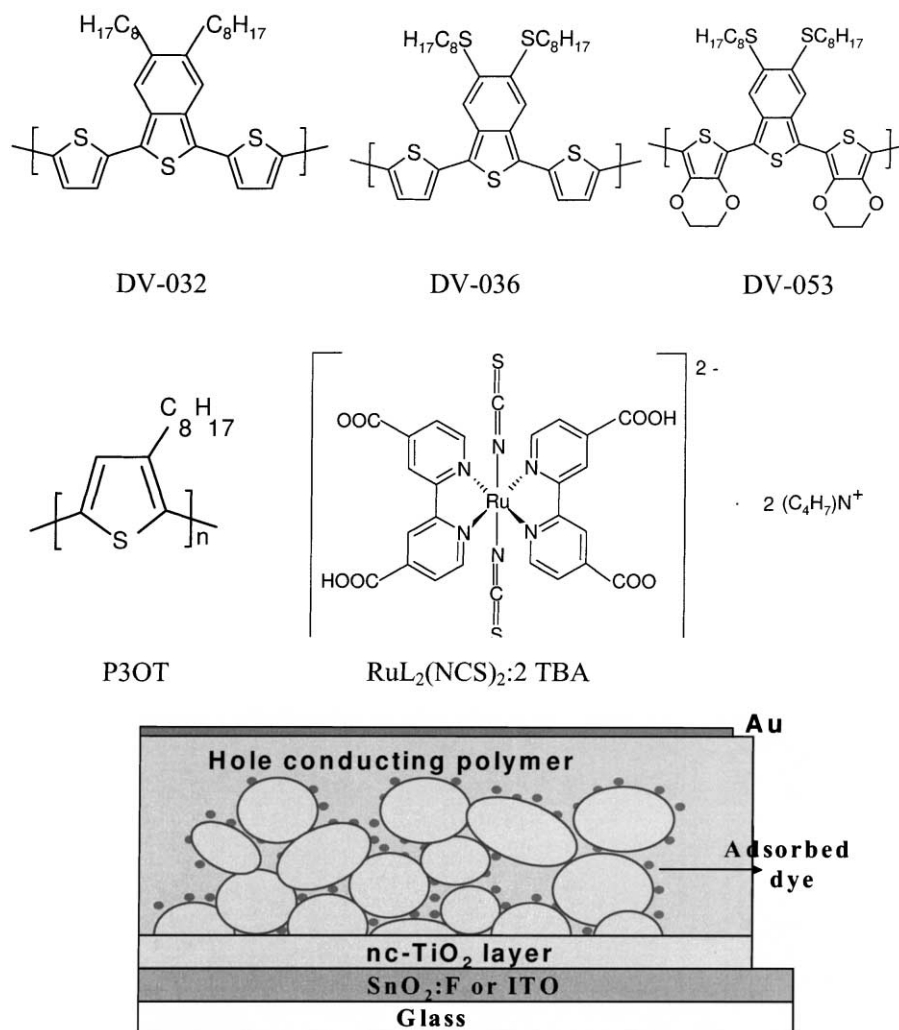


Fig. 1. Schematic diagram of the device configuration and molecular structures of the materials used.

(Switzerland)). Films of nanocrystalline TiO₂ on ITO (sheet resistance of 12–15 Ω/sq) or SnO₂:F coated glass substrates (sheet resistance of 13 Ω/sq) were prepared by doctor blading a TiO₂ paste from Solaronix Co. (Ti-nanoxide T, colloidal anatase particle size about 13 nm). The deposition process itself was performed by casting a given volume of 10 μl/cm² of TiO₂ paste by a rigid squeegee (microscope slide with polished edge). A slow drying step of the solvent and a following sintering process (heating from 70 to 450°C at a rate of 5°C/min and keeping at 450°C for 30 min to burn out the organic additives and to insure electrical contact between the TiO₂ particles) followed successively. The *cis*-bis(isothiocyanato)bis(2,2'-bipyridyl-4,4'-dicarboxylato)-ruthenium(II)bis-tetrabutylammonium, RuL₂(NCS)₂:2 TBA dye was used as sensitizer for the sintered TiO₂ film layers. The transparent TiO₂ layers were immersed for 2 days in a solution of the ruthenium dye (10 mg in 50 ml ethanol). The dye-coated TiO₂ films were then rinsed with pure ethanol and dried under nitrogen flow. Subsequently, the thin hole transport layer was coated by spin-coating either films of P3OT from toluene solution (10 mg in 1 ml

toluene) or films of composite PDTI/PMMA (9:1 weight ratio) from toluene solutions (10 mg in 1 ml toluene). The low molecular weight PDTIs were blended with an inert polymer matrix PMMA in order to enhance the film forming properties. After an additional drying step the gold (Au) top electrode was vacuum deposited. The thickness of the highly transparent nanocrystalline TiO₂ layer was approximately 2 μm while the thickness of the hole-transporting layer on top of the TiO₂ was typically in the range of 100–200 nm, as determined by Dektak measurements.

All cells were produced under ambient conditions. The current–voltage (*I/V*) characteristics are measured with a Keithley SMU 2400 source measurement unit in argon atmosphere under illumination through the ITO or SnO₂:F side by white light from a solar simulator (solar constant 575 with AM 1.5 filter, K.H. Steuernagel Lichttechnik GmbH) with an intensity of 80 mW/cm². The incident light intensity was measured using an AM 1.5 calibrated single-crystal Si photodiode. The temperature of the sample during measurement was 50°C. Spectrally resolved photocurrent measurements were recorded by Lock-In technique, illuminating the

device with $\sim 0.1 \text{ mW/cm}^2$ monochromatized light from a Xe arc lamp and white light background illumination and referencing them to a spectrally calibrated Si photodiode. The surface network morphology of these film layers was examined with an atomic force microscope in contact mode (Nanoscope IIIa from Digital Instruments).

3. Results and discussion

All solar cells were produced in sandwich geometry between two metal electrodes with different work functions (ITO: 4.5–4.9 eV [41,42] and Au: 5.1–5.4 eV [42,43]). In the present device configuration we chose gold as the top electrode material because its work function is close to the highest occupied molecular orbital (HOMO) of the hole conductors P3OT and PDTI [40]. Thus, hole injection from the polymeric organic materials into the metal electrode is energetically possible. In such a device configuration, the

TiO_2 conduction band electrons and the holes in the HTM are subsequently transported by electronic conduction to the contact electrodes and the dye is regenerated by hole injection into the HTM [32].

Fig. 2 shows a schematic energy level diagram for an $\text{SnO}_2\text{:F/nc-TiO}_2\text{/Ru-dye/P3OT/Au}$ (Fig. 2(a)) and $\text{SnO}_2\text{:F/nc-TiO}_2\text{/Ru-dye/PDTI/Au}$ (Fig. 2(b)) of the three-layered devices. In these three-layered devices, short circuit conditions

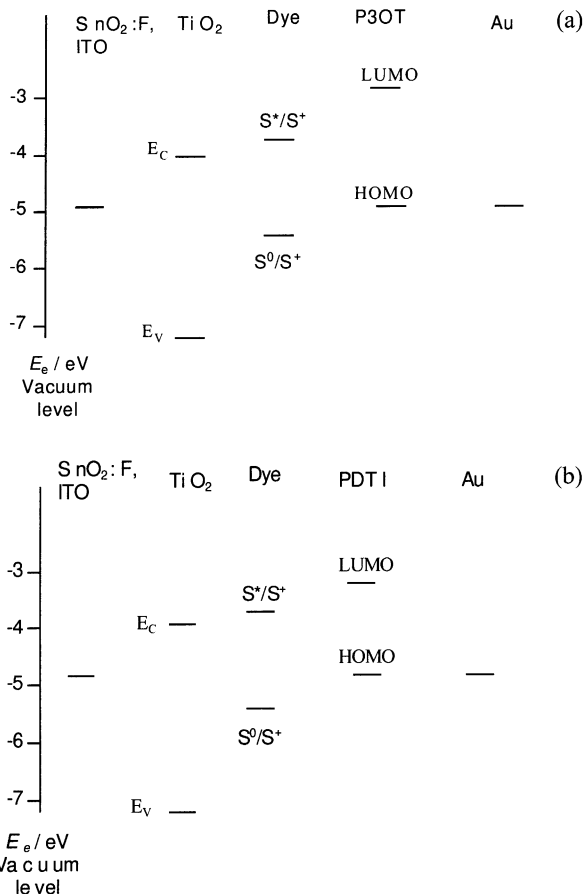


Fig. 2. Potential energy diagrams relative to vacuum level depicting the transfer of charge carriers for the (a) $\text{SnO}_2\text{:F/nc-TiO}_2\text{/Ru-dye/P3OT/Au}$ and (b) $\text{SnO}_2\text{:F/nc-TiO}_2\text{/Ru-dye/PDTI/Au}$ devices, where CB and VB is conduction and valence band of the TiO_2 nanocrystals; S_0/S^+ and S^*/S^+ is the ground and excited state potential of the ruthenium dye; LUMO and HOMO is the lowest unoccupied and the highest occupied molecular orbital of P3OT and PDTI, and work function levels of $\text{SnO}_2\text{:F}$ or ITO and Au.

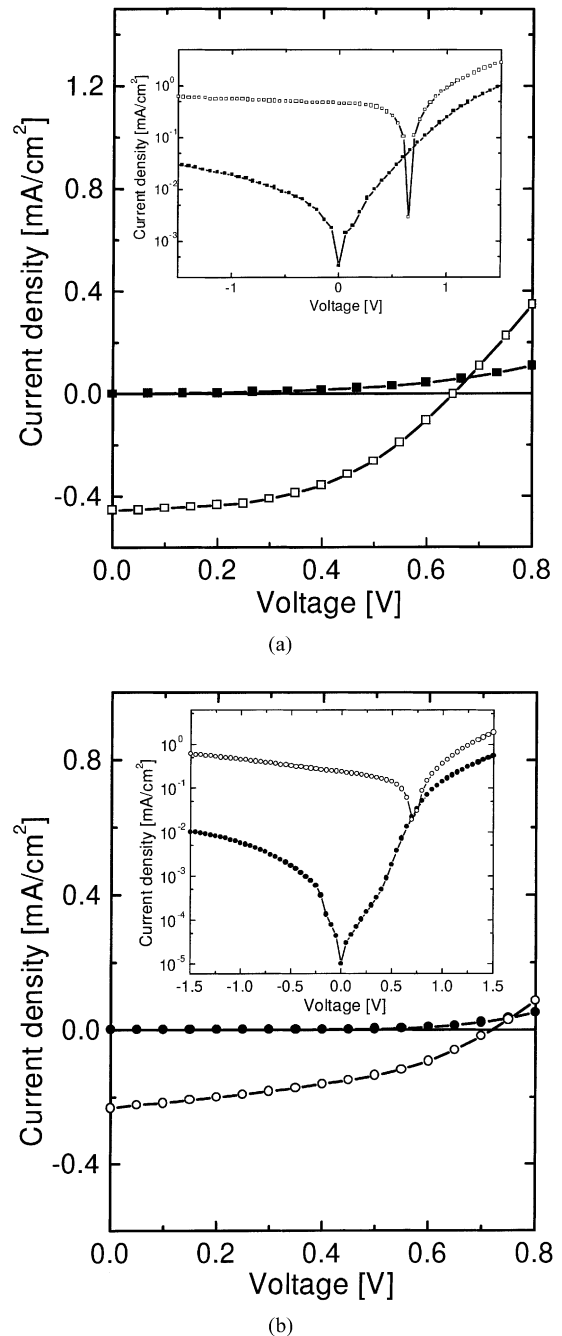


Fig. 3. I/V characteristics comparison of (a) $\text{SnO}_2\text{:F/nc-TiO}_2\text{/Ru-dye/P3OT/Au}$ (solid squares: dark, open squares: illuminated with 80 mW/cm^2) and (b) $\text{ITO/nc-TiO}_2\text{/P3OT/Au}$ (solid circles: dark, open circles: illuminated with 80 mW/cm^2) of hybrid solar cells in a linear scale. The inset is a logarithmic plot of the I/V data.

require the electron injection from the excited dye molecule into conduction band of TiO_2 and transfer of the hole to the Au back contact electrode. The bilayer device concept was demonstrated here by combining the electron transport properties of nanocrystalline TiO_2 and the light-absorbing and hole-transporting properties of the conjugated polymer, P3OT. Since all the above charge transfer processes are energetically favorable (see Fig. 2), current may be generated in the diode under illumination. In solid state dye-sensitized nanoporous TiO_2 solar cells, the anode and the cathode serve only as quasi-ohmic contacts and the maximum open circuit voltage (V_{oc}) is determined by the

difference between the quasi-Fermi level of the TiO_2 under illumination (~ 4.2 eV) and the HOMO of p-conductor [44]. The overall energy conversion efficiency, η_e has been calculated using the equation

$$\eta_e = \left(\frac{V_{oc} I_{sc} FF}{P_{inc}} \right)$$

under different intensities, where V_{oc} (V), I_{sc} (A/cm^2), FF and P_{inc} (W/cm^2) are the open circuit potential, short circuit current, fill factor and incident light power, respectively. We determine the value of the fill factor of the device, FF, by calculating the area of the maximum power rectangular area

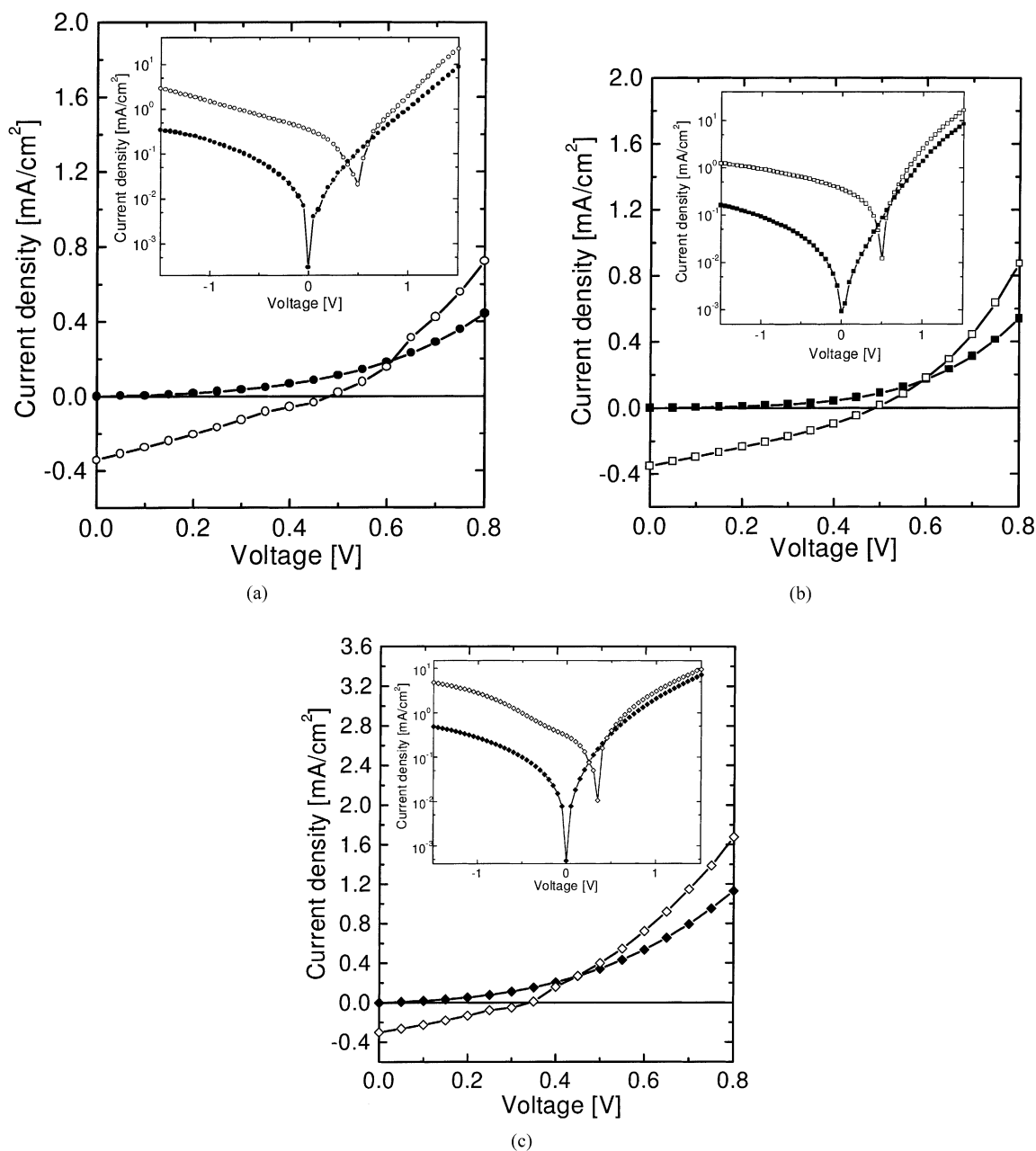


Fig. 4. I/V characteristics comparison of (a) ITO/nc- TiO_2 /Ru-dye/DV-032/Au (solid circles: dark, open circles: illuminated with $80 \text{ mW}/\text{cm}^2$); (b) ITO/nc- TiO_2 /Ru-dye/DV-036/Au (solid squares: dark, open squares: illuminated with $80 \text{ mW}/\text{cm}^2$); (c) ITO/nc- TiO_2 /Ru-dye/DV-053/Au (solid diamonds: dark, open diamonds: illuminated with $80 \text{ mW}/\text{cm}^2$) of hybrid solar cells in a linear scale. The inset is a logarithmic plot of the I/V data.

under the I/V curve in the fourth quadrant. Therefore, the filling factor is given by

$$FF = \frac{V_{\max} I_{\max}}{V_{oc} I_{sc}}$$

where V_{\max} and I_{\max} are voltage and current at the point of maximum power output.

The performance of photovoltaic devices from $\text{SnO}_2:\text{F}/\text{nc-TiO}_2/\text{Ru-dye}/\text{P3OT}/\text{Au}$ and $\text{ITO}/\text{nc-TiO}_2/\text{P3OT}/\text{Au}$ are compared and discussed in Fig. 3(a) and (b) by plotting the I/V characteristics in a linear and logarithmic scale, respectively. Because of the logarithmic scale of the current axis, the absolute value of the current is plotted against the voltage. The characteristic values of the device in Fig. 3(a) are $V_{oc} \sim 650$ mV, $I_{sc} \sim 450 \mu\text{A}/\text{cm}^2$ and a fill factor $FF \sim 0.44$ under white light illumination with $80 \text{ mW}/\text{cm}^2$. The rectification of this device is ~ 15 at ± 1.5 V in the dark. The power characteristics of the device without the dye (Fig. 3(b)) are $V_{oc} \sim 700$ mV, $I_{sc} \sim 230 \mu\text{A}/\text{cm}^2$ and a fill factor $FF \sim 0.37$ under white light illumination with $80 \text{ mW}/\text{cm}^2$. The rectification of this device is ~ 17 at ± 1.5 V in the dark. For $\text{SnO}_2:\text{F}/\text{nc-TiO}_2/\text{Ru-dye}/\text{P3OT}/\text{Au}$ device at $+1.5$ V a photocurrent of $\sim 3 \text{ mA}/\text{cm}^2$ and a dark current of $\sim 1 \text{ mA}/\text{cm}^2$ are observed, while for $\text{ITO}/\text{nc-TiO}_2/\text{P3OT}/\text{Au}$ device at $+1.5$ V a photocurrent of ca. $2 \text{ mA}/\text{cm}^2$ and a dark current of ca. $0.5 \text{ mA}/\text{cm}^2$ are measured. This indicates that the photoconductivity plays an important role for these devices at higher forward bias.

The overall energy conversion efficiency, η_e for the $\text{nc-TiO}_2/\text{Ru-dye}/\text{P3OT}$ and $\text{nc-TiO}_2/\text{P3OT}$ solid state hybrid solar cells was calculated with 0.16 and 0.08% under white light solar simulator $80 \text{ mW}/\text{cm}^2$, respectively.

In Fig. 4, the comparative I/V characteristics of (a) $\text{ITO}/\text{nc-TiO}_2/\text{Ru-dye}/\text{DV-032}/\text{Au}$; (b) $\text{ITO}/\text{nc-TiO}_2/\text{Ru-dye}/\text{DV-036}/\text{Au}$; and (c) $\text{ITO}/\text{nc-TiO}_2/\text{Ru-dye}/\text{DV-053}/\text{Au}$ solar cell devices are plotted in a linear and logarithmic scale. The characteristic data of the device in Fig. 4(a) (DV-032 as transport layer) are an open circuit voltage of ~ 500 mV, a short circuit current of approximately $340 \mu\text{A}/\text{cm}^2$ and a FF of 0.27 under white light illumination with $80 \text{ mW}/\text{cm}^2$. The rectification of this device in the dark at ± 1.5 V is ~ 14 . Furthermore, for the device in Fig. 4(b) (DV-036 as transport layer), an open circuit voltage of ~ 500 mV, a short circuit current of approximately $360 \mu\text{A}/\text{cm}^2$ and a FF of 0.35 under white light illumination with $80 \text{ mW}/\text{cm}^2$ are observed. The rectification of this device in the dark at ± 1.5 V is also ~ 16 . Open circuit voltages as high as 600 mV were observed for these devices. For the $\text{ITO}/\text{nc-TiO}_2/\text{Ru-dye}/\text{DV-053}/\text{Au}$ device slightly lower values are observed ($V_{oc} \sim 350$ mV, $I_{sc} \sim 300 \mu\text{A}/\text{cm}^2$, rectification ~ 10 at ± 1.5 V and a FF ~ 0.25). The lower V_{oc} might be due to the smaller band-gap ($E_g \sim 1.2$ eV) of the DV-053 copolymer, whereas the DV-032 and DV-036 copolymers have a E_g of 1.50 and 1.41 eV, respectively [40]. For $\text{ITO}/\text{nc-TiO}_2/\text{Ru-dye}/\text{DV-032}/\text{Au}$ and $\text{ITO}/\text{nc-TiO}_2/\text{Ru-dye}/\text{DV-036}/\text{Au}$ devices photocurrents of ~ 16 , $\sim 47 \text{ mA}/\text{cm}^2$ and dark

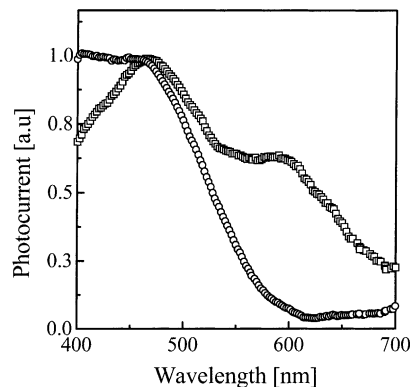


Fig. 5. The normalized photocurrent spectral response of $\text{P3OT}/\text{nc-TiO}_2$ (open circles) and $\text{P3OT}/\text{Ru-dye}/\text{nc-TiO}_2$ (open squares) devices.

currents of ~ 8.5 , $\sim 8 \text{ mA}/\text{cm}^2$ are observed at $+1.5$ V, respectively, while for $\text{ITO}/\text{nc-TiO}_2/\text{Ru-dye}/\text{DV-053}/\text{Au}$ device at $+1.5$ V a photocurrent of ca. $9 \text{ mA}/\text{cm}^2$ and a dark current of ca. $6 \text{ mA}/\text{cm}^2$ is recorded.

For the $\text{ITO}/\text{nc-TiO}_2/\text{Ru-dye}/\text{DV-036}/\text{Au}$, $\text{ITO}/\text{nc-TiO}_2/\text{Ru-dye}/\text{DV-032}/\text{Au}$ and $\text{ITO}/\text{nc-TiO}_2/\text{Ru-dye}/\text{DV-053}/\text{Au}$ hybrid solid state solar cells (under white light solar simulator $80 \text{ mW}/\text{cm}^2$) an overall energy conversion efficiency, $\eta_e \sim 0.08$, ~ 0.06 , and $\sim 0.03\%$ was calculated, respectively. These efficiency values are more than one order of magnitude smaller than the one observed for devices with a liquid electrolyte as transport medium. The origin of these low efficiencies has to origin in transport problems, since the charge injection from the Ru-dye to the TiO_2 should be comparable in devices with a polymer as hole conductor instead of an electrolyte. Since the conjugated polymers are known as good hole conductors, which can carry current densities of several mA/cm^2 in plastic solar cells [48], it is plausible to assume, that the transfer of the charge from the Ru-dye to the conjugated polymer is the limiting step,

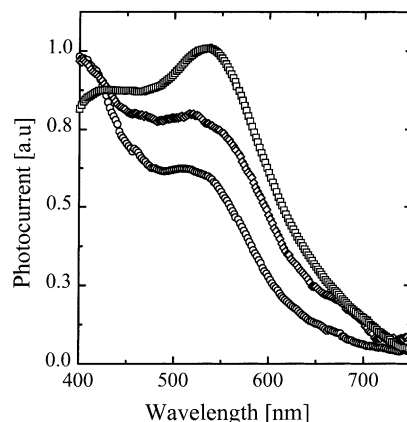


Fig. 6. The normalized spectrally resolved photocurrent of $\text{DV-053}/\text{Ru-dye}/\text{nc-TiO}_2$ (open squares), $\text{DV-032}/\text{Ru-dye}/\text{nc-TiO}_2$ (open circles) and $\text{DV-036}/\text{Ru-dye}/\text{nc-TiO}_2$ (open diamonds) hybrid solid state dye-sensitized solar cells.

probably due to poor filling or adhesion properties of the polymer.

Fig. 5 represents the normalized, but spectrally corrected photocurrent action spectrum of P3OT/nc-TiO₂ (open squares) and P3OT/Ru-dye/nc-TiO₂ (open circles) devices. For the bilayer device, the maximum of the spectral photocurrent is observed at ~470 nm and is assigned to the photoactivity of P3OT, although it is slightly blue-shifted to the absorption maximum of P3OT [45], which is usually

observed at ~500 nm. The three-layer device with the Ru-dye [2,46] shows two features, one around 470 nm which again is assigned to absorption of P3OT and a shoulder around 600 nm. The origin of this shoulder is not clear, since the contribution of the Ru-dye to the photocurrent is usually observed between 525 and 545 nm [47]. However, the shape of the action spectra obtained for RuL2(NCS)2:2 TBA may be strongly influenced by the nc-TiO₂ film thickness, the morphology and the absorption of the polymer layer [2].

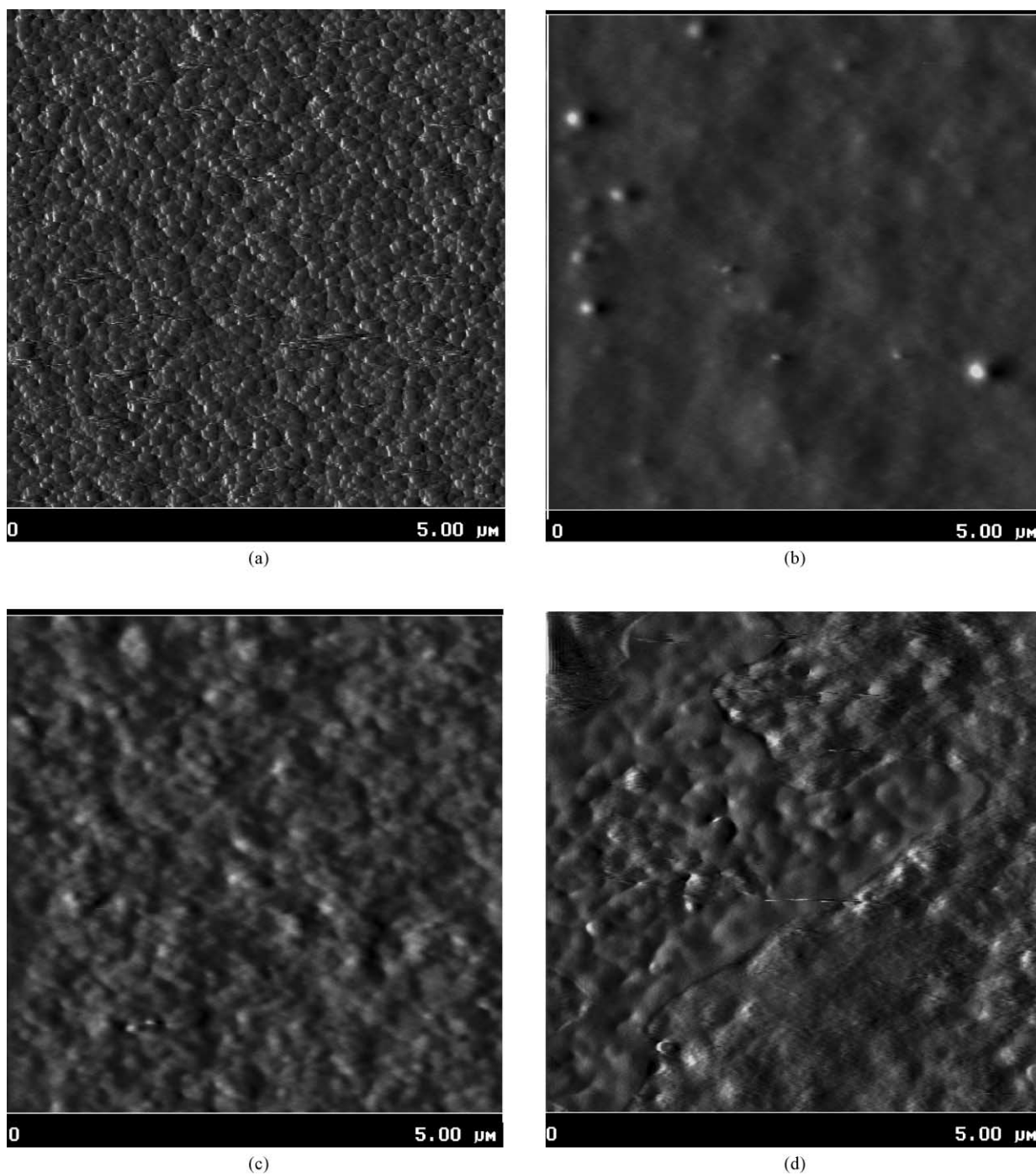


Fig. 7. AFM images of (a) nc-TiO₂; (b) nc-TiO₂/Ru-dye/P3OT; (c) TiO₂/P3OT; (d) nc-TiO₂/Ru-dye/DV-032; (e) nc-TiO₂/Ru-dye/DV-036; (f) nc-TiO₂/Ru-dye/DV-053 film layers.

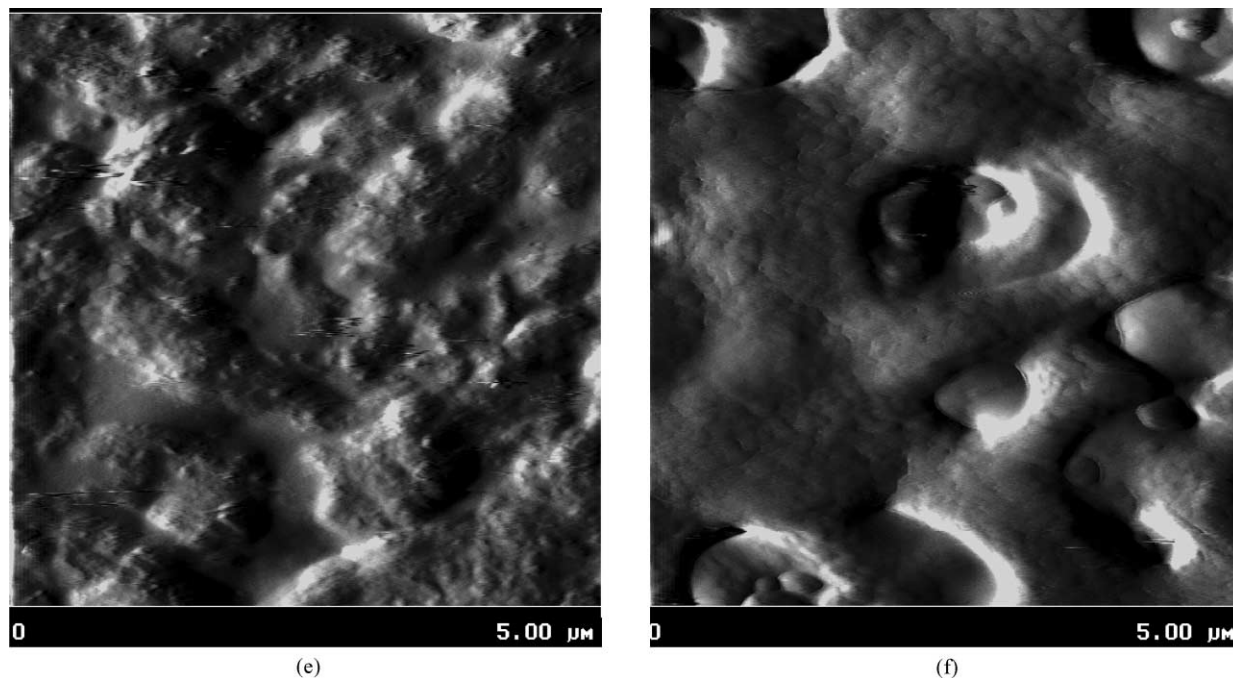


Fig. 7. (Continued).

Fig. 6 shows the normalized spectrally resolved photocurrent of DV-053/Ru-dye/nc-TiO₂ (open squares), DV-032/Ru-dye/nc-TiO₂ (open circles) and DV-036/Ru-dye/nc-TiO₂ (open diamonds) hybrid solid state dye-sensitized solar cells. For all three polymers a comparable onset of the photocurrent spectra is observed and the maximum of the photocurrent is between 515 and 535 nm. Thus, in Fig. 6, it can be noted that the photocurrent spectral response is correspondingly very close to the absorption spectrum of the RuL2(NCS)2:2 TBA (500–540 nm).

Fig. 7 illustrates the surface morphology of (a) nc-TiO₂; (b) nc-TiO₂/Ru-dye/P3OT; (c) nc-TiO₂/P3OT; (d) nc-TiO₂/Ru-dye/DV-032; (e) nc-TiO₂/Ru-dye/DV-036; and (f) nc-TiO₂/Ru-dye/DV-053 films as determined by atomic force microscope in the contact mode. According to AFM images, the nanostructured TiO₂ electrode in Fig. 7(a) is composed of interconnected and sub-micrometer sized TiO₂ particles and micropores. It has been observed that the TiO₂ particles in the film are uniform (root mean square surface roughness about 7.2 ± 2.2 nm) with an average diameter of 50 nm, which is much larger than the size of the particle in colloidal anatase solution (about 13 nm). Also, the average diameter of the pore sizes is around 50 nm. The nc-TiO₂/Ru-dye/P3OT films show a very homogeneous surface (RMS surface roughness of about 4.4 ± 0.8 nm) without pores or pinholes. In contrast, Fig. 7(c) suggests a less smooth surface for nc-TiO₂/P3OT films with RMS surface roughness of about 6 ± 0.85 nm. The surface properties of the PDTI-based devices are qualitatively comparable to the nc-TiO₂/P3OT devices, only the average surface roughness is higher. The nc-TiO₂/Ru-dye/DV-032 and nc-TiO₂/Ru-dye/DV-036 films have a RMS surface roughness of about 21.0 ± 5.2 nm and

25.5 ± 5.2 nm, whereas for the nc-TiO₂/Ru-dye/DV-053 films a RMS value of $\sim 32.0 \pm 3.5$ nm is observed.

From comparison of the surface properties of the TiO₂ layer with the one of the polymer coated TiO₂ layers, the AFM pictures indicate that the surface of the TiO₂ network is in all cases completely covered by the polymer layer. The good coverage of the polymer layer on top of the TiO₂ does not allow to evaluate the thickness of the layer and consequently, no information is gained on the filling of the TiO₂ network. Depending on the coating properties of the polymers, the mean surface roughness varies between ~ 7 nm for the P3OT films and 20–30 nm for the PDTI films. These values are significantly higher than for thin films processed on bare ITO glasses, where the surface roughness of the polymers is in the 1–2 nm range. Obviously, the surface roughness of the TiO₂ exerts a considerable influence onto the thin film properties of the spin-coated polymer films. Nevertheless, deep pin holes or large area defects are not detected for the polymer films on top of the TiO₂ and therefore shunts should be no major problem of the PV devices which is in good agreement with the results from *I/V* measurements.

4. Conclusion

We have realized hybrid solid state solar cells fabricated from inorganic nanoparticles as electron transporting material and an organic hole transport materials with photoexcited dye molecules as absorber and electron injector material. These devices show open circuit voltages up to 650 mV and short circuit currents up to $450 \mu\text{A}/\text{cm}^2$ under

AM 1.5 simulated solar radiation with 80 mW/cm². Under these illumination conditions the highest overall energy conversion efficiency, η_e , was found with 0.16% for the device consisting of nc-TiO₂/Ru-dye/P3OT/Au. By that, the efficiencies of the solid state devices are more than one order of magnitude lower in efficiency compared to devices where an electrolyte solution is responsible for hole transport. Several challenging scientific and technological problems remain to be solved. The major problems associated with solid state cells seem to be the imperfect topological filling of a polymeric hole conductor into the pores between the nanoparticles together with the adhesion of the polymer on the TiO₂ or on the Ru-dye. Further optimization of the complicated interpenetrating network structure for the three components (organic dye, polymeric hole conductor, inorganic nc-TiO₂) is expected to enhance the efficiencies.

Acknowledgements

This work was performed within the Christian Doppler Society's dedicated Laboratory for Plastic Solar Cells funded by the Austrian Ministry of Economic Affairs and Quantum Solar Energy Linz GmbH financial support from Austrian Foundation for Advancement of Science (FWF P12680 CHE), the "Magistrat Linz" and the "Land Oberösterreich" via the ETP are gratefully acknowledged. D. Gebeyehu is financed by the Austrian Academic Exchange Office (ÖAD) graduate scholarship program.

References

- [1] B. O'Regan, M. Grätzel, *Nature* 353 (1991) 737.
- [2] M.K. Nazeeruddin, A. Kay, I. Rodicio, R. Humphry-Baker, E. Müller, P. Liska, N. Vlachopoulos, M. Grätzel, *J. Am. Chem. Soc.* 115 (1993) 6382.
- [3] C.J. Barbé, F. Arendse, P. Comte, M. Jirousek, F. Lenzmann, V. Shklover, M. Grätzel, *J. Am. Ceram. Soc.* 80 (1997) 3157.
- [4] M.A. Green, K. Emery, K. Bücher, D.L. King, S. Igari, *Prog. Photovolt. Res. Appl.* 6 (1998) 35.
- [5] A. Kay, M. Grätzel, *J. Phys. Chem.* 97 (1993) 6272.
- [6] C.A. Bignozzi, R. Argazzi, M.T. Indelli, F. Scandola, *Sol. Energy Mater. Sol. Cells* 32 (1994) 229.
- [7] R. Argazzi, C.A. Bignozzi, T.A. Heimer, F.N. Castellano, G.J. Meyer, *Inorg. Chem.* 33 (1994) 5741.
- [8] M. Grätzel, D. Fraser, S.M. Zakeeruddin, M.K. Nazeeruddin, US Patent 5,393,903 (1995).
- [9] T.A. Heimer, S.T. D'Arcangelis, F. Frazad, J.M. Stipkala, G.J. Meyer, *Inorg. Chem.* 35 (1996) 5319.
- [10] H. Yanagi, S. Chen, P.A. Lee, K.W. Nebesny, N.R. Armstrong, A. Fujishima, *J. Phys. Chem.* 100 (1996) 5447.
- [11] M.K. Nazeeruddin, P. Péchy, M. Grätzel, *Chem. Commun.* 1705 (1997).
- [12] M.K. Nazeeruddin, E. Müller, R. Humphry-Baker, N. Vlachopoulos, M. Grätzel, *J. Chem. Soc., Dalton Trans.* 5471 (1997).
- [13] S.M. Zakeeruddin, M.K. Nazeeruddin, P. Péchy, F.P. Rotzinger, R. Humphry-Baker, K. Kalyanasundaram, M. Grätzel, V. Shklover, T. Haibach, *Inorg. Chem.* 36 (1997) 5937.
- [14] S. Ruile, O. Kohle, P. Péchy, M. Grätzel, *Inorg. Chim. Acta* 261 (1997) 129.
- [15] G.J. Meyer, *J. Chem. Educ.* 74 (1997) 652.
- [16] J. He, J. Zhao, T. Shen, H. Hidaka, N. Sepone, *J. Phys. Chem. B* 101 (1997) 9027.
- [17] S. Ferrere, B.A. Gregg, *J. Phys. Chem. B* 101 (1997) 4490.
- [18] S. Ferrere, B.A. Gregg, *J. Am. Chem. Soc.* 120 (1998) 843.
- [19] V. Balzani, S. Campagna, G. Denti, A. Juris, S. Serroni, M. Venturi, *Acc. Chem. Res.* 31 (1998) 26.
- [20] A. Usami, *Chem. Phys. Lett.* 277 (1997) 105.
- [21] J. Ferber, J. Luther, *Sol. Energy Mater. Sol. Cells* 54 (1998) 265.
- [22] S.Y. Huang, G. Schlichthörl, A.J. Nozik, M. Grätzel, A.J. Frank, *J. Phys. Chem. B* 101 (1997) 2576.
- [23] G. Schlichthörl, S.Y. Huang, J. Sprague, A.J. Frank, *J. Phys. Chem. B* 101 (1997) 8141.
- [24] L. Kavan, M. Grätzel, J. Rathousky, A. Zukal, *J. Electrochem. Soc.* 143 (1996) 394.
- [25] N. Papageorgiou, C. Barbé, M. Grätzel, *J. Phys. Chem. B* 102 (1998) 4156.
- [26] F. Cao, G. Oskam, P.C. Searson, *J. Phys. Chem.* 99 (1995) 17071.
- [27] K. Tennakone, G.R.R.A. Kumara, A.R. Kumarasinghe, K.G.U. Wijayantha, P.M. Sirimanne, *Sci. Technol.* 10 (1995) 1689.
- [28] K. Tennakone, G.R.R.A. Kumara, I.R.M. Kottegoda, K.G.U. Wijayantha, V.P.S. Perera, *J. Phys. D: Appl. Phys.* 31 (1998) 1492.
- [29] B. O'Regan, D.T. Schwartz, *Chem. Mater.* 7 (1995) 1349.
- [30] J. Hagen, W. Schaffrath, P. Otschik, R. Fink, A. Bacher, H.-W. Schmidt, D. Haarer, *Synth. Met.* 89 (1997) 215.
- [31] K. Murakoshi, R. Kure, Y. Wada, S. Yanagida, *Chem. Lett.* (1997).
- [32] U. Bach, D. Lupo, P. Comte, J.E. Moser, F. Weissörtel, J. Salbeck, H. Spreitzer, M. Grätzel, *Nature* 395 (1998) 583.
- [33] T.J. Savenije, J.M. Warman, A. Goossens, *Chem. Phys. Lett.* 287 (1998) 148.
- [34] T.J. Savenije, M.J.W. Vermeulen, M.P. de Hass, J.M. Warman, *Sol. Energy Mater. Sol. Cells* 61 (2000) 9.
- [35] J.J.M. Halls, K. Pichler, R.H. Friend, S.C. Moratti, A.B. Holmes, *Appl. Phys. Lett.* 68 (1996) 3120.
- [36] N.S. Sariciftci, *Primary Photoexcitations in Conjugated Polymers: Molecular Exciton Versus Semiconductor Band Model*, World Scientific Publishers, Singapore, 1998.
- [37] N. Greenham, X.G. Peng, A.P. Alivisatos, *Phys. Rev. B* 54 (1997) 17628.
- [38] K. Kajihara, K. Tanaka, K. Hirao, N. Soga, *Jpn. Appl. Phys.* 36 (1997) 5537.
- [39] P.A. Van Hal, M.P.T. Christiaans, M.M. Wienk, J.M. Kroon, R.A.J. Janssen, *J. Phys. Chem. B* 103 (1999) 4352.
- [40] R. Kiebooms, P. Adriaensens, D. Vanderzande, J. Gelan, *J. Org. Chem.* 62 (1997) 1473.
- [41] Y. Park, V. Choong, Y. Gao, B.R. Hsieh, C.W. Tang, *Appl. Phys. Lett.* 68 (1996) 2699.
- [42] I.D. Parker, *J. Appl. Phys.* 75 (1994) 1656.
- [43] I.H. Campbell, D.L. Smith, *Appl. Phys. Lett.* 74 (4) (1999) 561.
- [44] A.C. Arango, S.A. Carter, P.J. Brock, *Appl. Phys. Lett.* 74 (1999) 1698.
- [45] D. Gebeyehu, F. Padinger, C.J. Brabec, T. Fromherz, J.C. Hummelen, N.S. Sariciftci, *Intern. J. Photoenergy* 1 (2) (1999) 95.
- [46] M. Grätzel, *Platinum Metals Rev.* 38 (4) (1994) 151.
- [47] D. Gebeyehu, F. Padinger, C.J. Brabec, T. Fromherz, J.C. Hummelen, N.S. Sariciftci, *Int. J. Photoenergy* 1 (1999) 89–93.
- [48] S.E. Shaheen, C.J. Brabec, F. Padinger, T. Fromherz, J.C. Hummelen, N.S. Sariciftci, *Appl. Phys. Lett.* 78 (2001) 841–843.